

HPC: Hierarchical Point-based Latent Representation for Streaming Dynamic Gaussian Splatting Compression

Yangzhi Ma, Bojun Liu, Wenting Liao, Dong Liu, *Senior Member, IEEE*
 Zhu Li, *Senior Member, IEEE*, and Li Li[†], *Senior Member, IEEE*,

Abstract—While dynamic Gaussian Splatting has driven significant advances in free-viewpoint video, maintaining its rendering quality with a small memory footprint for efficient streaming transmission still presents an ongoing challenge. Existing streaming dynamic Gaussian Splatting compression methods typically leverage a latent representation to drive the neural network for predicting Gaussian residuals between frames. Their core latent representations can be categorized into structured grid-based and unstructured point-based paradigms. However, the former incurs significant parameter redundancy by inevitably modeling unoccupied space, while the latter suffers from limited compactness as it fails to exploit local correlations. To relieve these limitations, we propose HPC, a novel streaming dynamic Gaussian Splatting compression framework. It employs a hierarchical point-based latent representation that operates on a per-Gaussian basis to avoid parameter redundancy in unoccupied space. Guided by a tailored aggregation scheme, these latent points achieve high compactness with low spatial redundancy. To improve compression efficiency, we further undertake the first investigation to compress neural networks for streaming dynamic Gaussian Splatting through mining and exploiting the inter-frame correlation of parameters. Combined with latent compression, this forms a fully end-to-end compression framework. Comprehensive experimental evaluations demonstrate that HPC substantially outperforms state-of-the-art methods. It achieves a storage reduction of 67% against its baseline while maintaining high reconstruction fidelity.

Index Terms—Dynamic Gaussian Splatting Compression, Free-viewpoint Video, Latent Representation

I. INTRODUCTION

WITH the advent of immersive media, Free-Viewpoint Video (FVV) technology, which provides real-time viewing from arbitrary perspectives, has played a pivotal role in driving the evolution of next-generation media systems. An efficient, high-quality FVV framework has the potential to unlock a variety of applications, such as virtual reality (VR) and augmented reality (AR). For this purpose, prior works have investigated various scene representations, which involve meshes, point clouds, and radiance fields.

Among these candidates, the recently emerged 3D Gaussian Splatting (3DGS) [1] is opening up substantial new avenues

Y. Ma, B. Liu, W. Liao, D. Liu and L. Li are with Moe Key Laboratory of Brain-inspired Intelligent Perception and Cognition, University of Science and Technology of China, Hefei 230027, China (e-mail: mayz@mail.ustc.edu.cn; liubj@mail.ustc.edu.cn; liaowenting@mail.ustc.edu.cn; dongeliu@mail.ustc.edu.cn; lili1@mail.ustc.edu.cn.)

Z. Li is with the University of Missouri, Kansas City. (e-mail: lizhu@umkc.edu)

[†] denotes the corresponding author.

for FVV application. This representation excels at handling complex visual content while supporting real-time rendering. To meet the low-latency demands of real-time video applications, such as streaming media and immersive live broadcasting, pioneering works have extended 3DGS into an online-optimized dynamic framework [2]–[5]. These frameworks incrementally optimize the inter-frame deformation on a per-frame basis, thus facilitating the on-the-fly reconstruction. However, despite their essential advantages, the substantial size of the dynamic Gaussian Splatting representation poses significant challenges for streaming transmission. To this end, integrating compression into dynamic Gaussian Splatting has become a key research focus.

In the context of compression, a prevalent strategy for dynamic Gaussians employs a latent representation coupled with several neural networks for prediction [6]–[9]. The latent representation and neural networks are jointly optimized, compressed, and transmitted. Within this framework, the design of the latent representation emerges as one of the central challenges. Drawing inspiration from its success in earlier radiance field studies, the structural latent grid [10], [11] has been introduced to Gaussian Splatting [2], [6]–[8], [12]. Within this representation, the learnable latent embeddings are allocated to the vertices of the structural grid to generate a full-space latent field. During inference, the field is queried at the positions of individual Gaussians to retrieve their corresponding latent embeddings. However, assigning latent embeddings across the entire space incurs a prohibitive parameter explosion, rendering it impractical for direct optimization and storage. Therefore, such grid-based methods typically resort to either low-resolution grids [6] or hashing with collisions [2], [7], [8] to reduce parameters, which inevitably compromises the performance.

Alternatively, given that the positions of Gaussians constitute discrete sets occupying a vanishingly small fraction of the 3D space [13], it is naturally to attach a latent embedding directly to each point’s position, ignoring unoccupied areas. However, the existing point-based latent representation [9] primarily focuses on the isolated point, failing to model correlations within local neighborhoods and thus incurring spatial redundancy. Furthermore, given the non-uniform distribution of Gaussians, its single-scale design fails to capture the varied spatial characteristics, resulting in suboptimal performance.

In addition to the challenges in latent representation, another critical issue lies in the deficient compression strategy. Existing

studies [6]–[8] have devoted to compressing the latent representation through rate-aware optimization and entropy coding, but overlook the compression of the neural network parameters. This limitation not only prevents further bitrate reduction but also results in an imbalanced rate allocation between the latent and the network parameters. This creates a demand for an integrated framework that co-optimizes and compresses the latent representation alongside the neural network parameters.

In response to these limitations, we propose HPC, a novel streaming dynamic Gaussian Splatting framework that integrates a **Hierarchical Point-based** latent representation with a fully end-to-end **Compression** strategy. **On one hand**, our latent representation is built upon discrete points that operates on a per-Gaussian basis to avoid parameter redundancy in unoccupied space. To align with the non-uniform distribution of Gaussians, we equip the representation with multi-scale receptive fields via progressive downsampling, yielding the latent hierarchy. We further devise an aggregation scheme that incorporates both inner-scale and cross-scale processing to reduce spatial redundancy. It promotes local information sharing at multiple resolutions, thus achieving compactness. **On the other hand**, we undertake the first investigation into neural network compression for streaming dynamic Gaussian Splatting. Through an analysis of parameter distributions, we identify potential temporal redundancy between adjacent frames. Building on this observation, we derive a temporal reference strategy that leverages the latest decoded parameters to guide the optimization and compression of current-frame parameters. This strategy enables us to encode the energy-compact inter-frame residual rather than full parameters, significantly lowering the bitrate consumption. Unified with the compression of latent representation, our framework conducts a fully end-to-end optimization that balances the bitrate between the latent and network parameters, thereby attaining superior rate-distortion performance.

In summary, the proposed HPC offers the following key contributions:

- The HPC framework introduces a novel hierarchical latent point representation to match the inhomogeneous distribution of Gaussians while maintaining parameter efficiency. Spatial redundancy is effectively reduced via a dedicated aggregation mechanism that operates both within and across scales, promoting local information sharing and resulting in a compact representation.
- HPC pioneers the compression of network parameters in streaming dynamic Gaussian Splatting by exploiting inter-frame temporal redundancy. The resulting temporal reference strategy encodes compact residuals and is combined with latent compression in our fully end-to-end framework, enabling optimal bitrate allocation.
- Extensive experimental results demonstrate that HPC achieves a remarkable rate-distortion performance against state-of-the-art methods. Comprehensive ablations and analyses substantiate the effectiveness of each proposed component.

The remainder of this paper is structured as follows. Section II reviews related work in the relevant fields. The

preliminaries of our framework are provided in Section III. Sections IV and V detail the proposed HPC methodology. Experimental configurations and results are presented and analyzed in Section VI. Finally, Section VII concludes the paper.

II. RELATED WORK

A. Static Gaussian Splatting Compression

To address the substantial data footprint of 3DGS, Gaussian Splatting Compression seeks to eliminate redundancy from the Gaussian representations while preserving rendering fidelity. This section presents an overview of static Gaussian Splatting compression, covering two primary branches: post-training compression and generative compression.

Post-training compression decouples the compression process from the 3DGS training [14]–[19]. By directly operating on a pre-trained 3DGS model, it enables a fast compression pipeline without introducing additional optimization overhead. Existing post-training methods often leverage established transform [14] or encoding tools [15], [20].

For the optimal rate-distortion trade-off, generative compression methods perform joint training of compression and 3DGS representation [17], [21]–[32]. Some methods directly reduce the number of Gaussians by employing pruning [21], [22] or masking [23], [24] techniques to discard unimportant elements. Others apply vector quantization [23], [24], [26], [27] to reduce attribute-level redundancy. By leveraging the local spatial redundancy of 3DGS, Scaffold-GS [28] constructs a more efficient representation where a region of Gaussians is clustered to a few anchor points with an implicit representation, which drastically cuts down the storage count. Building upon Scaffold-GS, several works [29]–[32] take one more step to introduce dedicated entropy models and end-to-end rate-distortion optimization to achieve optimal performance.

B. Dynamic Gaussian Splatting Representation

Dynamic Gaussian Splatting extends 3DGS into the temporal domain to meet the demands of FVV applications. To accommodate diverse application requirements, mainstream representations can be broadly categorized into two paradigms: offline optimization and online optimization. The former takes an entire video sequence or multiple frames as its basic unit for both training and transmission, allowing it to leverage a richer temporal context for reference. The latter processes the individual frame as the basic unit. By modeling inter-frame changes incrementally on a per-frame basis, this approach naturally supports streaming applications.

For offline methods, one paradigm extends Gaussians into a 4D spatiotemporal domain, where each Gaussian captures a localized region in both space and time [33]–[38]. Another line of work basically applies the deformation to the canonical-space Gaussians [39]–[43]. However, these approaches face limitations in scenarios demanding streaming or involving long video sequences.

In contrast, online methods process 4D scenes in an iterative manner, adapting to changes on a frame-by-frame

basis to support streaming. Representations for online dynamic Gaussians fall into two main paradigms: the structured grid and the unstructured point representation. Following the former paradigms, 3DGStream [2] utilizes a hash-grid [10] to implicitly model inter-frame motion. Similarly, 4DGC [6] employs a latent grid for motion prediction, supplementing it with a compensation strategy to reduce information loss. iFVC [7] builds upon Scaffold-GS [28] and proposes a binary tri-plane for efficient residual prediction. However, since assigning features across the entire space incurs a prohibitive memory footprint, such representations are inherently limited by hash collisions [2], [7] or coarse resolution [6], resulting in suboptimal expressiveness.

In the point representation paradigm, parameters are directly attached to each Gaussian's position, thereby eliminating the parameter waste associated with unoccupied regions. Following this principle, HiCoM [3] optimizes the hierarchical coherent motion for efficient prediction. As the extension of HiCoM, ReCon-GS [4] introduces a dynamic hierarchy reconfiguration strategy for enhancement. ComGS [5] leverages a key-point motion model alongside a key-frame strategy, enabling efficient dynamic reconstruction. Despite their advantage of rapid training, these methods suffer from limited representational compactness, as they optimize and operate on the motion directly in the raw parameter space. Instead, another pathway is optimizing a latent representation, which relies on a neural network to learn the prediction of the motion or residual. Within this paradigm, QUEEN [9] operates by assigning a latent to each Gaussian and employs a jointly optimized latent decoder for residual inference. However, its per-point modeling scheme fails to capture correlations within local neighborhoods, incurring spatial redundancy. Moreover, its single-scale design is ill-suited to the non-uniformly distributed Gaussians, unable to adaptively capture spatial characteristics.

C. Compression of Dynamic Gaussian Splatting and Implicit Neural Video Representation

Following a similar taxonomy to its representation, compression for dynamic Gaussian Splatting can also be divided into two primary categories: offline and online. In offline methods, MEGA [37] achieves compression by decoupling color attributes and employing entropy-constrained deformation. While both GIFstream [42] and 4DGV [43] leverage established video codecs to achieve efficient compression.

Regarding online compression methods, QUEEN [9] quantizes the latent representation and then sparsifies the positional residuals via a learned gating module for storage saving. iFVC [7] quantizes its tri-plane latent embeddings in binary and leverages the empirical frequency distribution for entropy estimation, thereby facilitating end-to-end rate-distortion optimization. 4DGC [6] adopts a factorized entropy model [44] for both its motion grid and its compensated Gaussians. Building upon this, 4DGCP [8] specifically enables progressive streaming and real-time coding capabilities. Existing methods primarily focus on compressing the latent representation. A critical oversight, however, is that none of them jointly consider the neural network parameters. This

omission not only hinders further bitrate reduction but also leads to an inefficient bit allocation.

To bridge this gap, relevant insights can be adopted from the field of Implicit Neural Video Representation [45]–[50], where compressing the neural network itself has been a central research focus and offers well-established strategies. As a pioneer in this field, NeRV [45] applies pruning, quantization, and entropy coding directly to the neural network parameters. The follow-up methods [46], [47] integrate a rate estimation network for rate-aware training, and employ either statistical frequencies or a manually designed entropy model during inference. Zhang *et al.* [48] introduce a network-free entropy model by leveraging global statistics to ensure consistency between training and inference. To capture dependencies among network parameters, subsequent works [49], [50] introduce context-aware autoregressive modeling, which significantly enhances compression efficiency. Building on these insights, our goal is to design a neural network compression strategy tailored to the characteristics of dynamic Gaussian splatting and the demands of streaming. Combining with latent representation compression, we are aiming to build a fully end-to-end rate-distortion optimization framework.

III. PRELIMINARIES

A. 3D Gaussian Splatting

3DGS [1] achieves real-time, free-viewpoint rendering by combining a multitude of Gaussians with differentiable splatting and tile-based rasterization. Each Gaussian is parameterized by a set of attributes. Its spatial extent and shape are defined by a mean $\mu \in \mathbb{R}^3$ and a covariance matrix $\Sigma \in \mathbb{R}^{3 \times 3}$,

$$G(x) = \exp\left(-\frac{1}{2}(x - \mu)^\top \Sigma^{-1}(x - \mu)\right), \quad (1)$$

where $x \in \mathbb{R}^3$ is an arbitrary position in the 3D space, and Σ is constructed from a scaling matrix S and a rotation matrix R as $\Sigma = RSS^\top R^\top$. Following this, the rendered pixel color C is synthesized via α -blending, which composites these overlapping splats as follows:

$$C = \sum_{i \in \mathcal{N}} c^i \alpha^i \prod_{j=1}^{i-1} (1 - \alpha^j), \quad (2)$$

where \mathcal{N} is the set of sorted Gaussians contributing to the pixel, α^i is the opacity of the i -th Gaussian after projection, and c^i is its view-dependent color obtained from SH.

B. Neural Gaussian Representation

Scaffold-GS [28] enhances the compactness and fidelity of 3DGS by eliminating its local spatial redundancy through an implicit representation. It introduces Neural Gaussians \mathcal{NG} as the fundamental representation units that leverage a voxel-based clustering mechanism to manage the M local Gaussians. Each Neural Gaussian is defined by a set of attributes:

$$\mathcal{NG} = \{X \in \mathbb{R}^3, o \in \mathbb{R}^{3 \times M}, F \in \mathbb{R}^D, l \in \mathbb{R}^3\}, \quad (3)$$

where X denotes the location of the anchor obtained through voxelization, o represents the offsets of the M managed local

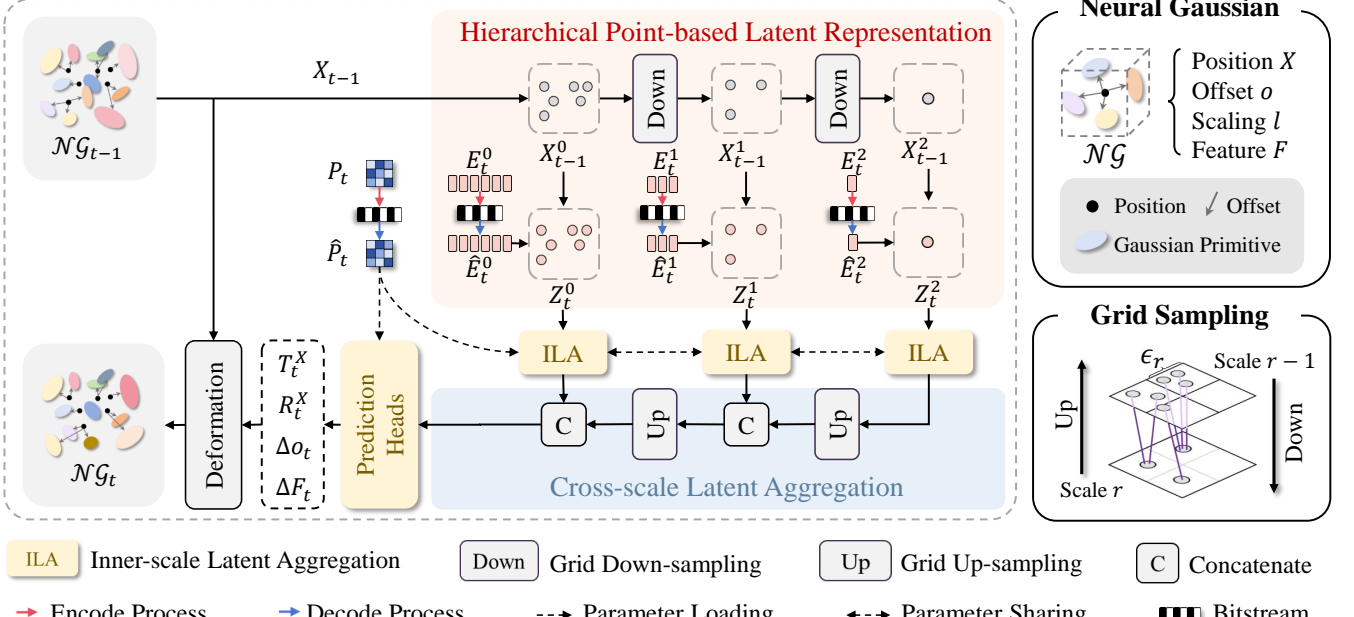


Fig. 1: Pipeline of the proposed HPC framework. The framework begins with the latest decoded Neural Gaussians \mathcal{NG}_{t-1} as a reference. It then constructs a hierarchical latent representation $\{Z_t^r\}_{r=0}^{L-1}$ (here, $L = 3$) by progressively down-sampling their positions into $\{X_{t-1}^r\}_{r=0}^{L-1}$ and pairing them with the decoded latent embeddings $\{\hat{E}_t^r\}_{r=0}^{L-1}$. After the Inner-scale Latent Aggregation (ILA) and Cross-scale Latent Aggregation (CLA), these latent points are fed into the prediction heads to obtain inter-frame residuals for deformation. In HPC, both the latent embeddings $\{E_t^r\}_{r=0}^{L-1}$ and network parameters P_t are compressed for transmission. We denote the reconstructed elements from the decoder with a hat mark.

Gaussians, and l is a scaling factor that regularizes their spatial distribution. Leveraging these attributes, the positions of the M local Gaussians can be computed as:

$$\{\mu^i\}_{i=0}^{M-1} = X + \{o^i\}_{i=0}^{M-1} \cdot l. \quad (4)$$

The remaining attributes of the local Gaussians are decoupled from the implicit feature F through several dedicated MLPs Φ_S , conditioned on the relative viewing information δ :

$$\{c^i, R^i, S^i, \alpha^i\}_{i=0}^{M-1} = \Phi_S(F, \delta). \quad (5)$$

IV. DYNAMIC GAUSSIAN REPRESENTATION

Building upon the success of Neural Gaussians for compressing static 3DGS scenes [29]–[31], we extend this representation to dynamic scenes by employing a sequence of Neural Gaussians $\{\mathcal{NG}_t\}_{t=0}^{T-1}$ as the scene representation for each frame, where t denotes the timestep, and T is the total frame number. Following the previous work [7], we leverage HAC [29] to generate compact \mathcal{NG}_0 for the initial frame.

The reconstruction pipeline of succeeding frames is illustrated in Fig. 1. Given a timestep t , we leverage the latest decoded Neural Gaussians \mathcal{NG}_{t-1} as the starting point. To model the temporal variations efficiently, a hierarchical point-based latent representation (Sec. IV-A) is constructed by progressively down-sampling the positions of \mathcal{NG}_{t-1} and pairing them with the learnable latent embeddings. To achieve compactness, the latent representation undergoes a two-stage aggregation process: inner-scale aggregation followed by cross-scale aggregation. Subsequently, the aggregated latent representation guides the deformation from \mathcal{NG}_{t-1} to \mathcal{NG}_t

(Sec. IV-B), reconstructing the scene of the current timestep through a motion affine transformation and feature compensation.

A. Hierarchical Point-based Latent Representation

To align with the inherently discrete and non-uniform spatial distribution of Neural Gaussians, we propose using a hierarchical point-based latent representation for inter-frame prediction. The construction of hierarchical latent points is illustrated in Fig. 1. We establish the spatial hierarchy by first initializing the finest scale from the primary positions as $X_{t-1}^0 = X_{t-1}$, then recursively obtaining coarser scales through grid sampling [51]:

$$X_{t-1}^r = \lfloor X_{t-1}^{r-1} / \epsilon^r + 0.5 \rfloor \cdot \epsilon^r, \quad r = 1, 2, \dots, L-1, \quad (6)$$

where r , ϵ , and L denote the scale index, grid size, and total scale count, respectively. For each resulting position X_{t-1}^r , we initialize a corresponding latent embedding E_t^r . After optimization, compression, and transmission, the decoder receives the reconstructed versions \hat{E}_t^r , which are then combined with the corresponding X_{t-1}^r to construct the the complete hierarchical latent points $\{Z_t^r = (X_{t-1}^r, \hat{E}_t^r)\}_{r=0}^{L-1}$. With this design, the latent points are feasible to capture local spatial character across different scales, enabling them to better capture the temporal dynamics of non-uniformly distributed Neural Gaussians while achieving compactness for efficient storage and transmission.

To this end, we leverage the established latent representation by progressively aggregating the latent points from the coarsest

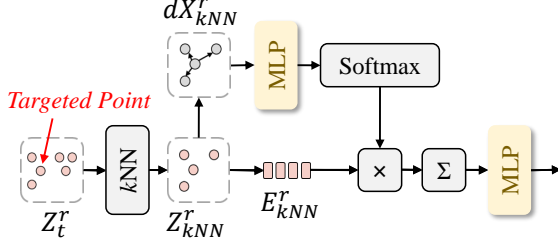


Fig. 2: Inner-scale Latent Aggregation (ILA). ILA takes a target point as input and locates its k -nearest neighbors. It then predicts aggregated weights from the relative positions, performs a weighted sum of the neighbor embeddings, and finally passes the result through an MLP to produce the output.

to the finest scale. We factorize this aggregation process into two complementary components: Inner-scale Latent Aggregation (ILA) and Cross-scale Latent Aggregation (CLA).

Inner-scale Latent Aggregation. Given the latent points $Z_t^r = (X_t^r, \hat{E}_t^r)$, the ILA module is designed to aggregate the embedding of a point’s neighbors to model local characteristics. As illustrated in Fig. 2, we first introduce the k NN algorithm to search for the k nearest neighbors for every single latent point. Following this, the relative positional offset dX_{kNN}^r between the target latent point and its neighbors is incorporated as auxiliary information to guide the aggregation. Specifically, these relative positions are fed into an MLP to predict per-neighbor aggregation weights which are normalized via softmax. The neighbor embeddings \hat{E}_{kNN}^r are then adaptively fused according to these weights. Ultimately, this fusion is passed through a final MLP to integrate information across all channels, producing the aggregated result. To reduce the parameter count, the ILA modules at different scales share the same set of parameters. Such an aggregation scheme facilitates interaction among neighboring latent points, promoting redundancy reduction and achieving spatial compactness.

Cross-scale Latent Aggregation. Building upon ILA, we next introduce the CLA process to fuse information across different resolutions. As illustrated in Fig. 1, CLA operates the inner-scale-aggregated latent points progressively from coarse to fine scales. At each step, coarse-scale embeddings are upsampled by copying them to their corresponding fine-scale positions, thereby recovering resolution. These upsampled points are then concatenated with the native fine-scale latent points to enable cross-scale fusion. Such a process is repeated recursively until the original resolution is reached, ultimately producing the cross-scale aggregated latent points for subsequent prediction. Through this CLA process, the aggregated latent representation integrates local spatial context captured across multiple receptive fields. Such a powerful context enables it to effectively model the underlying characteristics of non-uniformly distributed Neural Gaussians, thereby providing a superior foundation for subsequent prediction.

B. Dynamic Neural Gaussian Deformation

Within the aggregated latent points, we proceed to predict the Neural Gaussians $\mathcal{NG}_t = \{X_t, o_t, F_t, l_t\}$ for the cur-

rent timestep, conditioned on the previous state $\mathcal{NG}_{t-1} = \{X_{t-1}, o_{t-1}, F_{t-1}, l_{t-1}\}$. In this deformation, the scaling factor l is held constant as its variation has been proven to degrade performance [7], whereas X , o , and F are updated. Given this setup, the deformation is implemented via two complementary mechanisms: a residual compensation for the implicit feature and a motion affine transformation for geometric deformation.

Specifically, the aggregated latent points are first passed through the MLP-based prediction heads, yielding a set of deformation parameters: feature residual ΔF_t , anchor translation T_t^X , anchor rotation R_t^X , and offset residual Δo_t . For the implicit features, the compensation is achieved through adding the predicted residual ΔF_t :

$$F_t = F_{t-1} + \Delta F_t. \quad (7)$$

Geometric deformation is modeled by a motion affine transformation that combines global and local adjustments. This transformation updates the anchor position through translation T_t^X . Additionally, each local offset receives an extra individual adjustment Δo_t . To enable a more expressive geometric transformation, we adopt the strategy from [42] of applying a global rotation R_t^X to all corresponding offsets. Taken together, the complete update can be concisely expressed as:

$$X_t = X_{t-1} + T_t^X, \quad (8)$$

$$o_t = R_t^X(o_{t-1} + \Delta o_t). \quad (9)$$

Under such a mechanism, the Neural Gaussians gain sufficient expressive power to model temporal variation, enabling high-fidelity rendering through Neural Gaussian Splatting [28].

V. COMPRESSION SCHEME

A tailored compression scheme is integrated into HPC, aiming to fulfill the transmission requirements of streaming FFV. In our framework, the elements to be compressed and transmitted are the latent embedding $E_t = \{E_t^r\}_{r=0}^{L-1}$ (Sec. V-A) and the neural network parameters P_t (Sec. V-B). Especially, the compression of neural network parameters has been largely overlooked in streaming dynamic Gaussian Splatting, where existing methods [2], [6]–[9] simply transmit full-precision 32-bit floats. To bridge this gap and enhance rate-distortion efficiency, our work presents a novel scheme for compressing the streaming neural network parameters. Finally, we combine the compression of both parts and derive the overall rate-distortion objective to realize a fully end-to-end optimization (Sec. V-C).

A. Latent Embedding Compression

By virtue of the ILA and CLA design, the optimized latent embeddings E_t are compact with reduced spatial redundancy, ensuring they are well-suited for compression. As illustrated in Fig. 3 (a), the compression pipeline includes a quantization operation that discretizes the latent embeddings into integers, followed by an entropy coding module.

To circumvent the non-differentiability of quantization during training, we adopt the common practice from prior works [46]–[48] of employing distinct quantization proxies

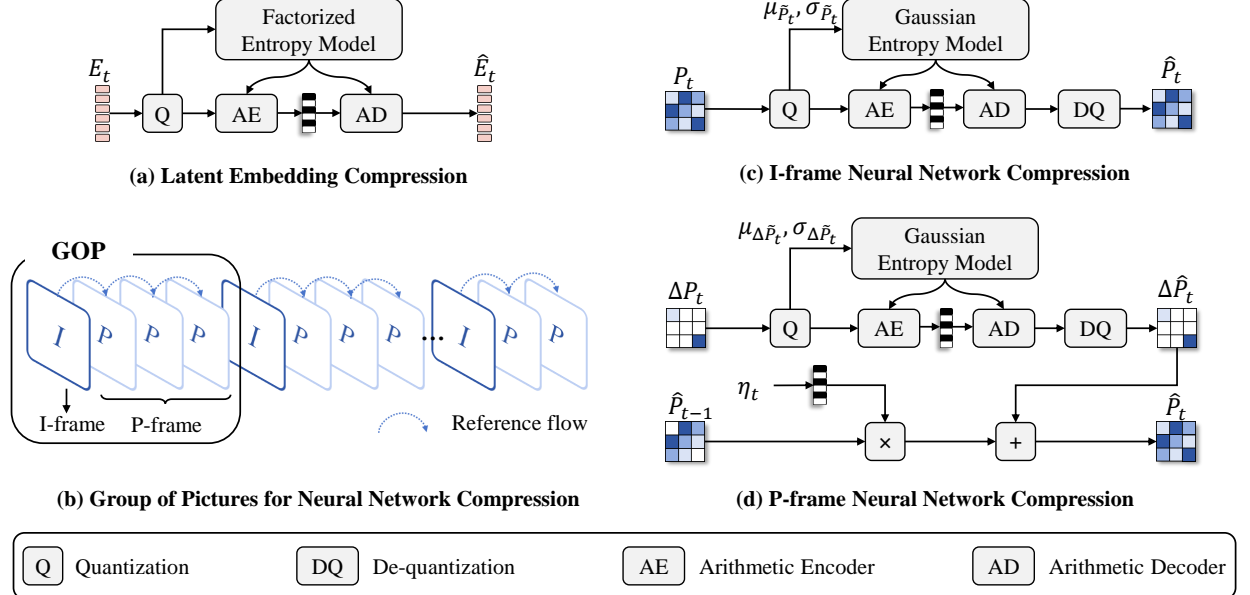


Fig. 3: HPC’s compression scheme. We incorporate compression for both the latent embeddings and the neural networks.

for distortion calculation and entropy estimation to obtain the quantized embedding \hat{E}_t . Specifically, the straight-through estimator (STE) is adopted for distortion calculation:

$$\hat{E}_t = \text{SG}(\lfloor E_t \rfloor - E_t) + E_t, \quad (10)$$

where $\text{SG}(\cdot)$ denotes the gradient-stopping operation. For entropy estimation, the rounding quantization is substituted with adding a uniform noise u :

$$\hat{E}_t = E_t + u, \quad u \sim \mathcal{U}\left(-\frac{1}{2}, \frac{1}{2}\right). \quad (11)$$

After quantization, the widely used factorized model [44] is adopted for entropy estimation. The entropy model comprises several learnable layers to progressively refine the input embedding to calculate their probabilities and bitrate:

$$p_{\text{PMF}}(\hat{E}_t) = p_{\text{CDF}}(\hat{E}_t + \frac{1}{2}) - p_{\text{CDF}}(\hat{E}_t - \frac{1}{2}), \quad (12)$$

$$\mathcal{R}(\hat{E}_t) = \mathbb{E}_{\hat{E}_t}[-\log_2 p_{\text{PMF}}(\hat{E}_t)], \quad (13)$$

where $p_{\text{PMF}}(\cdot)$ is the probability mass function, $p_{\text{CDF}}(\cdot)$ is the cumulative distribution function approximated by the factorized model, and $\mathcal{R}(\hat{E}_t)$ is the estimated bitrate of \hat{E}_t . Within the approximated probabilities, we can apply entropy coding for the latent embeddings to achieve further compression.

B. Neural Network Compression

To explore optimal compression of the neural networks in HPC, we start with analyzing the characteristics of their parameters. From the parameter distributions shown in Fig. 4, we observe that parameters in corresponding layers exhibit similar distribution between adjacent frames, while showing considerable differences across layers. This motivates us to leverage temporal context for redundancy reduction.

However, implementing such a naive strategy may introduce error propagation, where poorly optimized parameters in

one frame can adversely affect subsequent frames, resulting in cascading performance decline. Drawing inspiration from traditional video coding, we refer to the concept of Group of Pictures (GOP) [52] for an optimal reference structure. Specifically, as illustrated in Fig. 3 (b), a GOP typically comprises an Intra-coded frame (I-frame) and several Predictive-coded frames (P-frames). The I-frame, positioned at the GOP start, is independently optimized and compressed, while subsequent P-frames employ inter-prediction by referencing the preceding frame. By introducing a GOP structure with periodic insertion of independent I-frames, we prevent error propagation and maintain optimization stability over time.

I-frame Neural Network Compression. As illustrated in Fig. 3 (c), the compression pipeline for I-frames comprises quantization followed by entropy coding. Since the network parameters are particularly sensitive to quantization errors, we introduce a scaling operation prior to quantization to better preserve their precision:

$$\tilde{P}_t = \lfloor \frac{P_t - \min(P_t)}{\max(P_t) - \min(P_t)} \cdot (2^B - 1) \rfloor, \quad (14)$$

where \tilde{P}_t denotes the quantized and transmitted parameters, and B is the bit depth of quantization which controls the quantization precision. The minimum and maximum values of P_t are sent to the decoder as side information to obtain the reconstructed parameters \hat{P}_t :

$$\hat{P}_t = \tilde{P}_t \cdot [\max(P_t) - \min(P_t)]/(2^B - 1) + \min(P_t). \quad (15)$$

During training, we adopt the same proxy strategy used for latent embeddings: the STE for gradient propagation in the distortion term, and additive uniform noise for differentiable entropy estimation.

After quantization, entropy coding is applied to \tilde{P}_t for the final compression. Following [48], we introduce the network-free Gaussian distribution for entropy modeling, which is

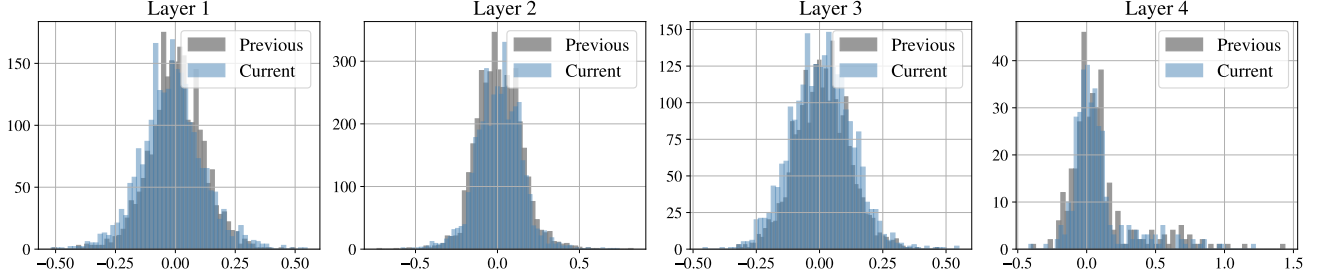


Fig. 4: Parameter distributions across adjacent frames in different layers.

parameterized solely by the statistical mean $\mu_{\tilde{P}_t}$ and variance $\sigma_{\tilde{P}_t}^2$. Consequently, the approximated probabilities $p_{\text{PMF}}(\tilde{P}_t)$ and bitrate $\mathcal{R}(\tilde{P}_t)$ are available as:

$$p_{\text{PMF}}(\tilde{P}_t) = \prod_i (\mathcal{N}(\mu_{\tilde{P}_t}, \sigma_{\tilde{P}_t}^2) * \mathcal{U}(-\frac{1}{2}, \frac{1}{2}))(\tilde{P}_t^i), \quad (16)$$

$$\mathcal{R}(\tilde{P}_t) = \mathbb{E}_{\tilde{P}_t}[-\log_2 p_{\text{PMF}}(\tilde{P}_t)], \quad (17)$$

where $*$ denotes convolution, and P_t^i denotes the each element in P_t . This design enables differentiable entropy estimation without introducing additional network parameters.

P-frame Neural Network Compression. For P-frames, we aim to exploit the decoded parameters from the previous frame \hat{P}_{t-1} as a contextual prior, which guides the optimization and compression of the current parameters. To this end, we draw upon the classical differential coding to optimize and encode the residual between consecutive frames, which exhibits greater energy compaction.

The P-frame neural network compression is illustrated in Fig. 3 (d). Specifically, inspired by the layer-wise temporal correlation shown in Fig. 4, we first introduce a learnable, per-layer scaling factor η_t to adapt \hat{P}_{t-1} for a coarse prediction of the current parameters. To bridge the remaining gap, we further optimize a per-parameter residual ΔP_t for fine-grained compensation. Both η_t and ΔP_t are transmitted to the decoder. Due to its minimal count, the per-layer η_t is preserved at the original precision without compression. In contrast, the per-parameter ΔP_t undergoes further compression for bitrate reduction. Within the received η_t and the decoded residuals $\hat{\Delta P}_t$, the final parameters \hat{P}_t can be reconstructed as follows:

$$\hat{P}_t = \eta_t \cdot \hat{P}_{t-1} + \Delta \hat{P}_t. \quad (18)$$

To compress the residuals ΔP_t , we apply a similar quantization strategy as used for the I-frame parameters. Here, we normalize the energy-compact residual ΔP_t by introducing the full parameter dynamic range derived from \hat{P}_{t-1} , ensuring the reconstructed parameter \hat{P}_t is represented at a consistent target precision while achieving bitrate savings:

$$v_{\min} = \min(\hat{P}_{t-1}, \Delta P_t), \quad v_{\max} = \max(\hat{P}_{t-1}, \Delta P_t). \quad (19)$$

$$\Delta \tilde{P}_t = \lfloor \frac{\Delta P_t - v_{\min}}{v_{\max} - v_{\min}} \cdot (2^B - 1) \rfloor, \quad (20)$$

$$\Delta \hat{P}_t = \Delta \tilde{P}_t \cdot (v_{\max} - v_{\min}) / (2^B - 1) + v_{\min}. \quad (21)$$

For further entropy calculation, we adopt the same strategy as the compression of I-frame parameters:

$$p_{\text{PMF}}(\Delta \tilde{P}_t) = \prod_i (\mathcal{N}(\mu_{\Delta \tilde{P}_t}, \sigma_{\Delta \tilde{P}_t}^2) * \mathcal{U}(-\frac{1}{2}, \frac{1}{2}))(\Delta \tilde{P}_t^i), \quad (22)$$

$$\mathcal{R}(\Delta \tilde{P}_t) = \mathbb{E}_{\Delta \tilde{P}_t}[-\log_2 p_{\text{PMF}}(\Delta \tilde{P}_t)]. \quad (23)$$

Within the proposed temporal reference strategy, the optimized residuals exhibit higher energy compactness. This leads to a lower transmission cost compared to encoding the full parameters, while still preserving the representational capacity of the neural network.

C. Rate-distortion Optimization

Finally, we jointly optimize the entire framework by minimizing a combined loss of the total estimated bitrate and the rendering distortion, pursuing the optimal rate-distortion performance in an end-to-end manner. Given a timestep t , we calculate the weighted sum of distortion loss $\mathcal{L}_{\mathcal{D}}^{(t)}$ and the rate loss $\mathcal{L}_{\mathcal{R}}^{(t)}$ as our overall supervision objective $\mathcal{L}^{(t)}$:

$$\mathcal{L}^{(t)} = \mathcal{L}_{\mathcal{R}}^{(t)} + \lambda \mathcal{L}_{\mathcal{D}}^{(t)}, \quad (24)$$

where λ is the Lagrange multiplier which controls the rate-distortion balance. Specifically, we adopt the 3DGS rendering loss [1] as the distortion term:

$$\mathcal{L}_{\mathcal{D}}^{(t)} = \mathcal{L}_1^{(t)} + \lambda_{\text{SSIM}} \mathcal{L}_{\text{SSIM}}^{(t)}. \quad (25)$$

For the rate term, we combined the estimated bitrate of both latent embeddings and neural network parameters:

$$\mathcal{L}_{\mathcal{R}}^{(t)} = \begin{cases} \mathcal{R}(\hat{E}_t) + \mathcal{R}(\tilde{P}_t), & t \bmod T_{\text{GOP}} = 0, \\ \mathcal{R}(\hat{E}_t) + \mathcal{R}(\Delta \tilde{P}_t), & t \bmod T_{\text{GOP}} \neq 0, \end{cases} \quad (26)$$

where T_{GOP} is the predefined size of a GOP.

VI. EXPERIMENTS

A. Experiment Setup

Datasets. We evaluate our method on two widely adopted FVV datasets: **(1) the N3DV dataset** [54], captured by a 21-camera rig, which comprises dynamic scenes at 2704×2028 and 30 FPS. **(2) the Meet Room dataset** [55], captured by a 13-camera system, comprising dynamic scenes at 1280×720 and 30 FPS. For each dataset, one camera view is held out for testing, and the rest are used for training.

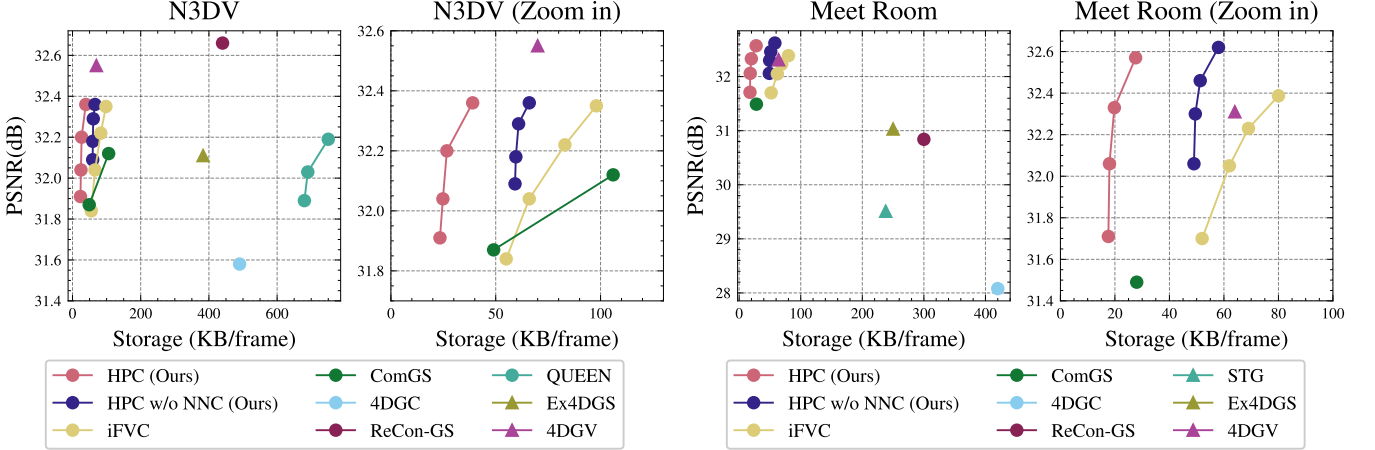


Fig. 5: Rate-distortion curves on the N3DV and the Meet Room datasets. Methods marked with \circ and \triangle respectively denote the online and offline optimized methods. Points and curves closer to the top-left corner indicate better performance.



Fig. 6: Qualitative comparisons on the *flame_steak* and *vrheadset*. For a fair comparison, we retrain all methods with the same initial sparse points, while iFVC [7] and HPC share the same initial-frame model.

Implementation Details. For the latent point hierarchy, we adopt the approach of ContextGS [30] to construct $L = 3$ scales, with the ratio of points between adjacent scales set to 0.2. The latent embeddings contain 16 channels per scale. In the ILA module, we set $k = 4$ for the k -NN search. For neural network compression, parameters are quantized to $B = 8$ bit depth. The GOP size T_{GOP} is set to 5. For training, λ is adjusted from 0.048 to 0.002 to achieve variable bitrate. We train HAC [29] as the initial frame for 15000 iterations following iFVC [7]. For the subsequent frames, we train our model for 500 iterations. We employ the torchac library [56] for arithmetic coding. All experiments are conducted on an NVIDIA GeForce RTX 3090 GPU.

Baselines. We evaluate the proposed HPC by comparing it with state-of-the-art online frameworks, including

3DGStream [2], HiCoM [3], iFVC [7], 4DGC [6], QUEEN [9], ComGS [5], 4DGCP [8], and ReCon-GS [4]. Several offline methods [34], [37], [42], [43], [53], which are optimized within multiple frames, are also included in the benchmark to serve as reference points for a more comprehensive performance assessment. As existing methods lack neural network compression, we introduce a corresponding baseline, HPC w/o NNC, by disabling this component in our full model. This allows it to be fairly compared against prior methods while isolating the contribution of our other components.

Metrics. We evaluate rate-distortion performance using Peak Signal-to-Noise Ratio (PSNR) and Structural Similarity Index Measure (SSIM) [57] as objective distortion metrics, with bitrate measured in kilobytes per frame (KB/frame). For a precise comparison of rate-distortion efficiency, we compute

TABLE I: Quantitative comparison. The online methods are organized, in order, into three categories: grid-based methods, existing point-based methods, and our methods, with horizontal lines separating each category. For methods with multiple rate-distortion points, we report both the lowest ($-l$) and highest ($-h$) quality results. The best and second-best results are highlighted in **Red** and **Orange** cells, respectively.

N3DV dataset				
Category	Method	PSNR (dB) \uparrow	SSIM \uparrow	Storage (KB/frame) \downarrow
Offline	STG [34]	32.05	-	666
	GIFStream [42]	31.75	0.938	33
	Ex4DGS [53]	32.11	0.94	383
	MEGA [37]	31.49	-	83
	4DGV [43]	32.55	-	70
Online	3DGStream [2]	31.69	0.948	7780
	4DGC [6]	31.58	0.943	500
	4DGCP [8]- l	30.68	0.926	210
	4DGCP [8]- h	31.64	0.944	640
	iFVC [7]- l	31.84	0.950	63
	iFVC [7]- h	32.35	0.953	99
	HiCoM [3]	31.17	-	900
	QUEEN [9]- l	31.89	0.946	680
	QUEEN [9]- h	32.19	0.946	750
	ComGS [5]- l	31.87	-	49
Online	ComGS [5]- h	32.12	-	106
	ReCon-GS [4]	32.66	0.957	440
	HPC w/o NNC- l (Ours)	32.22	0.953	59
	HPC w/o NNC- h (Ours)	32.36	0.955	66
	HPC- l (Ours)	31.91	0.951	23
Meet Room dataset	HPC- h (Ours)	32.36	0.955	39
Meet Room dataset				
Category	Method	PSNR (dB) \uparrow	SSIM \uparrow	Storage (KB/frame) \downarrow
Offline	STG [34]	29.51	0.932	238
	Ex4DGS [53]	31.03	0.946	250
	4DGV [43]	32.31	0.957	64
Online	3DGStream [2]	30.79	-	4100
	4DGC [6]	28.08	0.922	420
	iFVC [7]- l	32.05	0.956	63
	iFVC [7]- h	32.39	0.959	80
	HiCoM [3]	26.73	-	600
Online	ComGS [5]	31.49	-	28
	ReCon-GS [4]	30.84	0.954	300
	HPC w/o NNC- l (Ours)	32.26	0.959	52
	HPC w/o NNC- h (Ours)	32.62	0.962	61
	HPC- l (Ours)	31.71	0.957	18
Meet Room dataset	HPC- h (Ours)	32.57	0.961	28

the Bjontegaard Delta Bit-Rate (BD-BR) [58], which quantifies the bitrate savings at equivalent PSNR quality. Note that a negative BD-BR value indicates decreased storage at the same fidelity compared to the anchor method, which is desirable.

B. Comparison Results

Quantitative Comparisons. The qualitative comparison is elaborated in Table I. HPC achieves competitive reconstruction quality while requiring about 20 KB/frame at minimum for storage on both datasets, which is significantly lower than other online-optimized methods. By adjusting λ during training, HPC is able to achieve the best fidelity on the Meet

TABLE II: BD-BR (%) results against iFVC [7]. The results are tested on the N3DV and Meet Room datasets.

Method	N3DV	Meet Room	Average
iFVC [7]	0.0	0.0	0.0
HPC	-64.9	-70.7	-67.3
HPC w/o NNC	-27.1	-28.9	-28.0
HPC w/o ILA	-60.0	-66.7	-63.4
HPC w/o CLA	-45.9	-51.0	-48.5

Room dataset and the second-best on the N3DV dataset, while consuming less than 40 KB/frame for storage. Notably, the reconstruction fidelity is significantly influenced by the initial frame, which will be discussed in Sec. VI-D. Comprehensive, Fig. 5 shows the overall rate-distortion performance, where we can observe our HPC significantly surpasses previous state-of-the-art methods. For a fair comparison, we use iFVC [7], which shares the same initial frame with ours, as the anchor to calculate the BD-BR metric. As shown in Table. II, HPC achieves bitrate savings of 67.3% across the two datasets. Yet, even with neural network compression disabled, it delivers a 28% reduction in bitrate, which underscores the substantial contribution of its representation design.

We give a comprehensive analysis of the significant bitrate reduction. In contrast to methods like HiCoM [3], ComGS [5], and ReCon-GS [4], which directly optimize Gaussian attribute residuals, HPC adopts a different strategy: it optimizes a latent representation paired with a lightweight network to predict residuals. This implicit formulation allows entropy constraints to be applied properly, leading to high compactness and compression efficiency. Compared to approaches with the implicit dynamic model like iFVC [7], 4DGC [6], 4DGCP [8], and QUEEN [9], HPC develops a more compact and efficient latent representation. When combined with the neural network compression, this leads to greater overall performance gains.

Qualitative Comparisons. We conduct a qualitative comparison with 4DGC [6] and iFVC [7] on the *flame_steak* sequence and the *vrheadset* sequence. To ensure a fair comparison, all methods are initialized with the same sparse point cloud. Additionally, iFVC [7] and our HPC share an identical first-frame model. As shown in Fig. 6, HPC achieves the best reconstruction quality while attaining the smallest model size. Notably, HPC better preserves fine details, such as facial features, animal fur, and flame textures. Furthermore, it demonstrates superior capability in modeling components with large motions, including fast-moving arms and hands. These results indicate that HPC accurately captures dynamic scene elements, maintains high-fidelity details in complex objects, and achieves a highly compact representation.

C. Ablation Study

To assess the impact of individual components, we conduct comprehensive ablation studies. Specifically, our analysis is structured around the three main contributions: the latent representation, the latent aggregation scheme, and the neural network compression scheme.

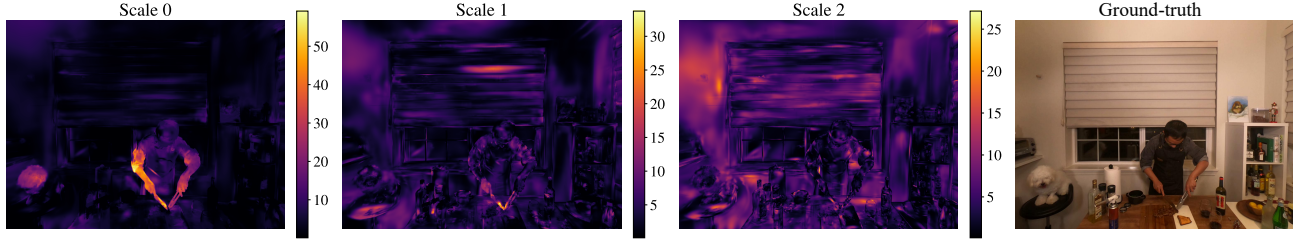


Fig. 7: Bit allocation of latent embeddings in different scales. This visualization maps the bitrate consumed by each latent embedding to a color value, which is then rendered onto a 2D image to show the bit allocation.

TABLE III: Ablation study of different latent representations on the N3DV dataset. Tri-plane is the anchor for BD-BR.

	Tri-plane	Hash-grid	Hierarchical points (Ours)
BD-BR (%) \downarrow	0.0	-6.7	-21.8

TABLE IV: Study on different bit depths of neural network quantization. The results are based on the Meet Room dataset with the highest bitrate.

Bit depth	PSNR (dB) \uparrow	Latent Storage (KB) \downarrow	Network Storage (KB) \downarrow	Total Storage (KB) \downarrow
32	32.62	16	42	58
16	32.60	16	21	37
8	32.57	16	10	26
4	7.31	60	5	65

Different Types of Representation. We first compare the proposed hierarchical latent point with two established structural representation: the hash-grid and the tri-plane. The hash-grid adopts the same configuration as in 3DGStream [2], while the tri-plane adopts the same configuration as in iFVC [7]. As summarized in Table III, the proposed hierarchical points representation achieves the best performance among the three candidates. This result demonstrates that our design achieves more efficient parameter allocation for discrete Gaussians compared to structural representations.

Latent Aggregation. We evaluate the proposed aggregation scheme by separately ablating the ILA and CLA modules as described in Table II. Equipped with the ILA module, our model yields an extra bitrate saving of 4%. This result confirms that the component effectively facilitates local information sharing, thereby reducing spatial redundancy. When evaluating the CLA module, it achieves an additional 20% bitrate saving, underscoring the effectiveness of the aggregated information from multi-resolution receptive fields. To further

TABLE V: Ablation study of neural network compression on the Meet Room dataset. M_0 is the anchor method for BD-BR calculation.

Method	M_0	M_1	M_2
Quantization	✓	✓	✓
Entropy constraint		✓	✓
Temporal reference			✓
BD-BR (%) \downarrow	0.0	-6.6	-14.6

demonstrate this, we visualize the bit allocation results in different scales. As observed in Fig. 7, the allocation exhibit significant variations across different scales. This indicates that the multi-scale representation successfully enables HPC to capture distinct features at different levels of granularity. The latent embeddings at the coarse scale are oriented toward capturing motion in large regions (e.g., the moving arm), while those at finer scales excel at modeling detailed variations. The aggregation of information across scales empowers HPC to model scenes more efficiently and comprehensively.

Neural Network Compression. Prior to compression, the parameters must first be quantized. To investigate its effect, we reduce the precision from the original 32 bits to several lower bit depths, including 16, 8, and 4 bits. As shown in Table IV, the storage cost of network parameters decreases linearly with the quantization bit depth. Compared to the original precision, reconstructions at 8 or 16 bits exhibit only marginal degradation (less than 1 dB). However, at 4-bit quantization, the training becomes unstable and diverges, leading to a significant drop in reconstruction quality. Concurrently, the excessive quantization of the factorized entropy model causes the increasing bitrate of the latent representation. Based on this analysis, we select 8-bit quantization as our operating point, which effectively minimizes storage overhead while preserving the essential neural network capability.

For further ablation study, we progressively incorporate other components into the baseline with 8-bit quantization, which is denoted as M_0 . As shown in Table V, to compress the parameters efficiently, we incorporate an entropy constraint into the parameter optimization, denoted as M_1 . This is implemented using the differentiable network-free Gaussian entropy model [48] to enable bitrate estimation and entropy coding, which yields a 6.6% performance gain.

Finally, we leverage temporal references across frames to exploit inter-frame correlations for redundancy reduction, denoted as M_2 . As visualized in Fig. 8, our temporal reference strategy enables the model to capture and transmit the energy-compact residual. This strategy achieves significant bitrate savings without compromising the network’s representational capacity. However, as shown in Fig. 9, a naive integration of the temporal reference model leads to severe error propagation, characterized by a continuous degradation in reconstruction quality with longer reference intervals. We therefore introduce the GOP reference structure and investigate the impact of its size. As observed in Fig. 9, compared to no inter-frame refer-

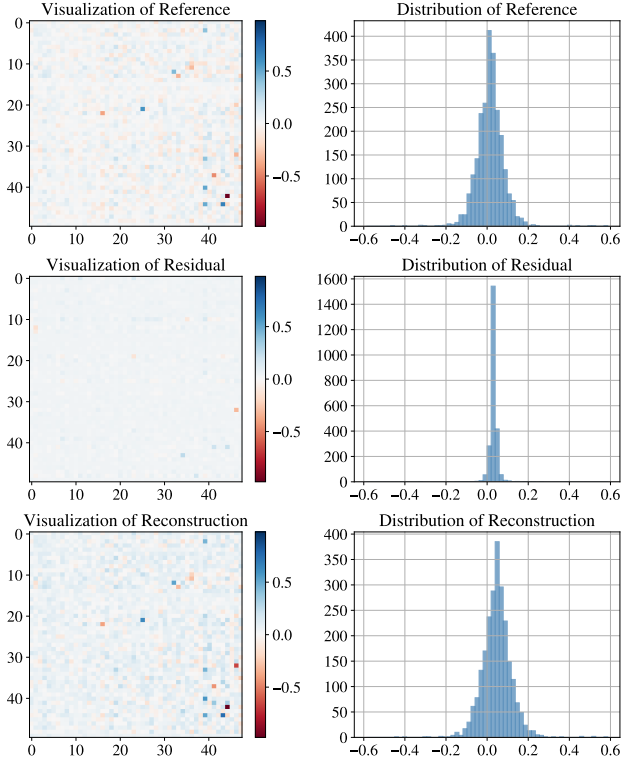


Fig. 8: Analysis of neural network parameters and residuals. The reconstructed parameters are calculated with the reference parameters and residuals following Eq. (18).

TABLE VI: Complexity comparison. The results are evaluated on an NVIDIA RTX 3090 GPU, with values averaged on both the N3DV and Meet Room datasets.

Method	Train (min)↓	Render (FPS)↑	Encode (s)↓	Decode (s)↓
4DGC [6]	0.83	184	0.70	0.11
iFVC [7]	0.17	140	0.10	0.09
HPC w/o NNC (Ours)	0.60	141	0.13	0.10
HPC (Ours)	1.01	140	0.33	0.18

encing (GOP size=1), larger GOP sizes consistently reduce the overall storage. In terms of reconstruction quality, GOP sizes of 10 and 20 still exhibit periodic degradation, compromising the overall performance. Empirically, a GOP size of 5 is selected as it not only reduces the bitrate but also yields a slight improvement in reconstruction quality. This quality gain stems from a beneficial optimization bias provided by the well-chosen temporal reference, which steers the network toward a better optimization direction and thereby strengthens its expressive power. With the GOP reference structure, our temporal reference strategy contributes a performance gain of 14.6% over the base model as shown in Table. V.

D. Analysis

Complexity. Table VI compares the complexity of our method against 4DGC [6] and iFVC [7] in terms of training time, rendering speed, encoding time, and decoding time. For training time, the extended duration of HPC is attributed to its

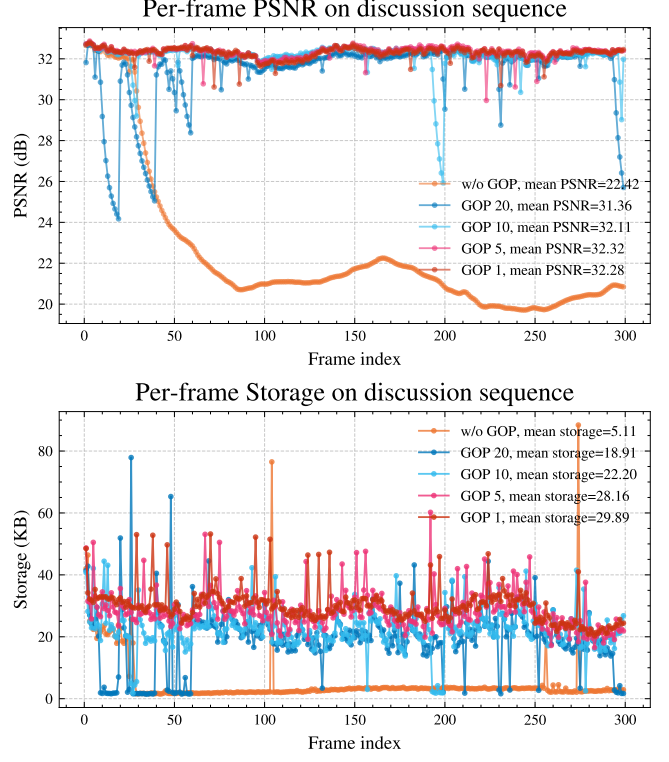


Fig. 9: Per-frame PSNR and storage on the *discussion* sequence across different GOP size.

rate-aware training scheme for network parameters, which introduces more complex gradient updates and thus slows the optimization. When the neural network compression module is removed, the training speed of HPC surpasses 4DGC [6] but remains slower than iFVC [7]. This is primarily due to the additional parameters in the introduced aggregation modules and entropy model, which in turn require more iterations for convergence. The rendering is slightly slower for both HPC and iFVC [7] due to the overhead of Neural Gaussian Splatting [28], whereas 4DGC [6] uses the faster, non-neural original splatting [1]. The longer overall coding time of HPC stems from its need to entropy encode both latent embeddings and network parameters, whereas the other two methods compress only the former. When focusing specifically on the shared task of encoding latent embeddings, HPC matches the coding speed of iFVC [7] and outperforms 4DGC [6].

Initial Frame Analysis. In streaming FVV, the initial frame critically influences all subsequent reconstruction. Given its pivotal role, we comprehensively evaluate our work by analyzing the operation and results for the initial frame across different methods as shown in Table VII.

There exists various of initial representations and training strategies across different methods. 3DGStream [2] adopts the vanilla 3DGS representation and training strategy for the initial frame. ReCon-GS [4] regularizes the training of 3DGS by injecting Gaussian noise into the position attributes to mitigate overfitting. In contrast to the vanilla 3DGS, both iFVC and our HPC adopt the HAC framework [29] to obtain a highly compressed Neural Gaussian [28] representation for the initial

TABLE VII: Analysis of the initial frame across different methods on N3DV. The average results across all frames are based on the highest bitrate.

Method	Representation	Init. training strategy	Init. Storage (KB)↓	Avg. Storage (KB)↓	Init. PSNR (dB)↑	Avg. PSNR (dB)↑	PSNR gain over Init. (%)↑
3DGStream [2]	Vanilla 3DGS	Vanilla 3DGS training	51660	7780	32.13	31.69	-1.36
ReCon-GS [4]	Vanilla 3DGS	Noise-injected 3DGS training	11120	440	32.75	32.66	-0.27
iFVC [7]	Neural Gaussian	HAC training	2480	99	32.21	32.35	+0.43
HPC (Ours)	Neural Gaussian	HAC training	2480	39	32.21	32.36	+0.46

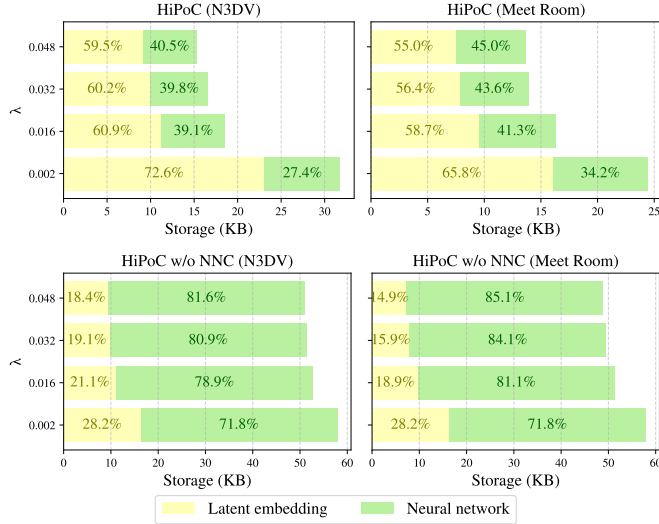


Fig. 10: Bit allocation between latent embedding and neural network.

frame. This approach achieves substantial storage savings ($20\times$ and $4.5\times$ reduction against 3DGStream [2] and ReCon-GS [4], respectively). In terms of reconstruction fidelity, the noise-injection strategy effectively prevents ReCon-GS [4] from overfitting to the training views, thus achieving the highest PSNR for both the initial and subsequent frames. However, we observe that using vanilla 3DGS [1] as the representation leads to a quality drop, whereas adopting Neural Gaussians [28] yields a consistent gain over the initial reconstruction quality. Among Neural Gaussian-based methods, our HPC achieves the highest PSNR gain of 0.46%, further proving its effectiveness.

Bit Allocation. To provide a comprehensive analysis of our method, we analyze the bit allocation results between the latent embedding and the neural network across different bitrates. As observed in Fig. 10, the rate allocation varies across different bitrate points. At lower bitrates, their allocated rates are comparable. As the total bitrate budget increases, the proportion allocated to the latent embeddings grows consistently and reaches approximately 70% at the highest bitrate.

When the neural network compression module is disabled, we observe that the bitrate share of the network parameters surges to over 80% across low and medium bitrate points. This high allocation not only impedes further bitrate reduction but also potentially constrains the model’s overall expressive capacity, demonstrating the necessity of compressing network

parameters.

VII. CONCLUSION AND FUTURE WORKS

We explore a hierarchical point-based latent representation tailored for dynamic Gaussian Splatting and introduce HPC. It ensures efficient parameter allocation, enables the effective capture of spatial correlations from non-uniformly distributed Gaussians, and ultimately delivers efficient, high-quality reconstruction. A fully end-to-end compression framework, which jointly optimizes both the latent representation and the neural network for an optimal rate-distortion trade-off, is designed to achieve significant bitrate savings. Extensive experiments demonstrate that HPC achieves the state-of-the-art compression performance against existing methods. Comprehensive studies analyze and demonstrate the effectiveness of its technical components. By achieving significant bitrate savings for dynamic Gaussian Splatting, our work paves the way for the field of streaming free-viewpoint video.

The primary limitation of HPC is its longer training duration and higher coding latency compared to competing methods due to the additional rate-aware optimization and compression for network parameters. Future work should incorporate lightweight designs to accelerate both the training and coding processes, thereby facilitating practical deployment.

REFERENCES

- [1] B. Kerbl, G. Kopanas, T. Leimkühler, and G. Drettakis, “3d gaussian splatting for real-time radiance field rendering.” *ACM Trans. Graph.*, vol. 42, no. 4, pp. 139–1, 2023.
- [2] J. Sun, H. Jiao, G. Li, Z. Zhang, L. Zhao, and W. Xing, “3dgstream: On-the-fly training of 3d gaussians for efficient streaming of photo-realistic free-viewpoint videos,” in *Proceedings of the IEEE/CVF Conference on Computer Vision and Pattern Recognition (CVPR)*, June 2024, pp. 20 675–20 685.
- [3] Q. Gao, J. Meng, C. Wen, J. Chen, and J. Zhang, “Hicom: Hierarchical coherent motion for dynamic streamable scenes with 3d gaussian splatting,” in *Advances in Neural Information Processing Systems (NeurIPS)*, 2024.
- [4] J. Fu, Q. Gao, C. Wen, Y. Wu, S. Ma, J. Zhang, and J. Zhang, “Recon-GS: Continuum-preserved gaussian streaming for fast and compact reconstruction of dynamic scenes,” in *The Thirty-ninth Annual Conference on Neural Information Processing Systems*, 2025.
- [5] J. Chen, Q. Mao, Y. Bao, X. MENG, F. Meng, R. Wang, and Y. Liang, “Motion matters: Compact gaussian streaming for free-viewpoint video reconstruction,” in *The Thirty-ninth Annual Conference on Neural Information Processing Systems*, 2025.
- [6] Q. Hu, Z. Zheng, H. Zhong, S. Fu, L. Song, X. Zhang, G. Zhai, and Y. Wang, “4dgc: Rate-aware 4d gaussian compression for efficient streamable free-viewpoint video,” in *Proceedings of the Computer Vision and Pattern Recognition Conference (CVPR)*, June 2025, pp. 875–885.
- [7] L. Tang, J. Yang, R. Peng, Y. Zhai, S. Shen, and R. Wang, “Compressing streamable free-viewpoint videos to 0.1 mb per frame,” in *Proceedings of the AAAI Conference on Artificial Intelligence*, vol. 39, no. 7, 2025, pp. 7257–7265.

[8] Z. Zheng, Z. Wu, H. Zhong, Y. Tian, N. Cao, L. Xu, J. Yao, X. Zhang, Q. Hu, and W. Zhang, “4DGCP: Efficient hierarchical 4d gaussian compression for progressive volumetric video streaming,” in *The Thirty-ninth Annual Conference on Neural Information Processing Systems*, 2025.

[9] S. Girish, T. Li, A. Mazumdar, A. Shrivastava, D. Luebke, and S. D. Mello, “QUEEN: QUantized efficient ENcoding for streaming free-viewpoint videos,” in *The Thirty-eighth Annual Conference on Neural Information Processing Systems*, 2024.

[10] T. Müller, A. Evans, C. Schied, and A. Keller, “Instant neural graphics primitives with a multiresolution hash encoding,” *ACM transactions on graphics (TOG)*, vol. 41, no. 4, pp. 1–15, 2022.

[11] S. Fridovich-Keil, G. Meanti, F. R. Warburg, B. Recht, and A. Kanazawa, “K-planes: Explicit radiance fields in space, time, and appearance,” in *Proceedings of the IEEE/CVF Conference on Computer Vision and Pattern Recognition*, 2023, pp. 12479–12488.

[12] H. Yu, W. Gong, J. Chen, and H. Ma, “Get3dgs: Generate 3d gaussians based on points deformation fields,” *IEEE Transactions on Circuits and Systems for Video Technology*, vol. 35, no. 5, pp. 4437–4449, 2025.

[13] Y. Ma, B. Liu, J. Li, L. Li, and D. Liu, “Hash grid feature pruning,” *arXiv preprint arXiv:2512.22882*, 2025.

[14] S. Xie, W. Zhang, C. Tang, Y. Bai, R. Lu, S. Ge, and Z. Wang, “Mesongs: Post-training compression of 3d gaussians via efficient attribute transformation,” in *European Conference on Computer Vision*. Springer, 2024, pp. 434–452.

[15] S. Lee, F. Shu, Y. Sanchez, T. Schierl, and C. Hellge, “Compression of 3d gaussian splatting with optimized feature planes and standard video codecs,” in *Proceedings of the IEEE/CVF International Conference on Computer Vision (ICCV)*, October 2025, pp. 25496–25505.

[16] S. Girish, K. Gupta, and A. Shrivastava, “Eagles: Efficient accelerated 3d gaussians with lightweight encodings,” in *European Conference on Computer Vision*, 2024, pp. 54–71.

[17] S. Li, C. Wu, H. Li, X. Gao, Y. Liao, and L. Yu, “Gscodec studio: A modular framework for gaussian splat compression,” *IEEE Transactions on Circuits and Systems for Video Technology*, pp. 1–1, 2026.

[18] Q. Yang, L. Yang, G. V. der Auwera, and Z. Li, “HybridGS: High-efficiency gaussian splatting data compression using dual-channel sparse representation and point cloud encoder,” in *Forty-second International Conference on Machine Learning*, 2025.

[19] Y. Wang, M. Liu, Q. Yang, H. Huang, L. Yang, and Y. Xu, “On the efficient adaptive streaming of 3d gaussian splatting over dynamic networks,” *IEEE Transactions on Circuits and Systems for Video Technology*, pp. 1–1, 2025.

[20] C. Wang, S. N. Sridhara, E. Pavez, A. Ortega, and C. Chang, “Adaptive voxelization for transform coding of 3d gaussian splatting data,” in *2025 IEEE International Conference on Image Processing (ICIP)*, 2025, pp. 2414–2419.

[21] M. S. Ali, M. Qamar, S.-H. Bae, and E. Tartaglione, “Trimming the fat: Efficient compression of 3d gaussian splats through pruning,” in *35th British Machine Vision Conference 2024, BMVC 2024, Glasgow, UK, November 25–28, 2024*. BMVA, 2024.

[22] Z. Fan, K. Wang, K. Wen, Z. Zhu, D. Xu, and Z. Wang, “Lightgaussian: unbounded 3d gaussian compression with 15x reduction and 200+ fps,” in *Proceedings of the 38th International Conference on Neural Information Processing Systems*, ser. NIPS ’24. Red Hook, NY, USA: Curran Associates Inc., 2024.

[23] H. Wang, H. Zhu, T. He, R. Feng, J. Deng, J. Bian, and Z. Chen, “End-to-end rate-distortion optimized 3d gaussian representation,” in *European Conference on Computer Vision*. Springer, 2024, pp. 76–92.

[24] J. C. Lee, D. Rho, X. Sun, J. H. Ko, and E. Park, “Compact 3d gaussian representation for radiance field,” in *2024 IEEE/CVF Conference on Computer Vision and Pattern Recognition (CVPR)*, 2024, pp. 21719–21728.

[25] X. Liu, X. Wu, P. Zhang, S. Wang, Z. Li, and S. Kwong, “Comp3d: Efficient 3d scene representation via compressed gaussian splatting,” in *Proceedings of the 32nd ACM International Conference on Multimedia*, 2024.

[26] K. Navaneet, K. P. Meibodi, S. A. Koohpayegani, and H. Pirsiavash, “Comp3d: Smaller and faster gaussian splatting with vector quantization,” *ECCV*, 2024.

[27] S. Niedermayr, J. Stumpfegger, and R. Westermann, “Compressed 3d gaussian splatting for accelerated novel view synthesis,” in *2024 IEEE/CVF Conference on Computer Vision and Pattern Recognition (CVPR)*, 2024, pp. 10349–10358.

[28] T. Lu, M. Yu, L. Xu, Y. Xiangli, L. Wang, D. Lin, and B. Dai, “Scaffold-gs: Structured 3d gaussians for view-adaptive rendering,” in *Proceedings of the IEEE/CVF Conference on Computer Vision and Pattern Recognition*, 2024, pp. 20654–20664.

[29] Y. Chen, Q. Wu, W. Lin, M. Harandi, and J. Cai, “Hac: Hash-grid assisted context for 3d gaussian splatting compression,” in *European Conference on Computer Vision*. Springer, 2024, pp. 422–438.

[30] Y. Wang, Z. Li, L. Guo, W. Yang, A. Kot, and B. Wen, “Context3dgs: Compact 3d gaussian splatting with anchor level context model,” *Advances in neural information processing systems*, vol. 37, pp. 51532–51551, 2024.

[31] Y.-T. Zhan, C.-Y. Ho, H. Yang, Y.-H. Chen, J. C. Chiang, Y.-L. Liu, and W.-H. Peng, “Cat-3dgs: A context-adaptive triplane approach to rate-distortion-optimized 3dgs compression,” in *The Thirteenth International Conference on Learning Representations*, 2025.

[32] Y. Chen, Q. Wu, W. Lin, M. Harandi, and J. Cai, “Hac++: Towards 100x compression of 3d gaussian splatting,” *IEEE Transactions on Pattern Analysis and Machine Intelligence*, vol. 47, no. 11, pp. 10210–10226, 2025.

[33] Y. Duan, F. Wei, Q. Dai, Y. He, W. Chen, and B. Chen, “4d-rotor gaussian splatting: Towards efficient novel view synthesis for dynamic scenes,” in *ACM SIGGRAPH 2024 Conference Papers*, ser. SIGGRAPH ’24. New York, NY, USA: Association for Computing Machinery, 2024.

[34] Z. Li, Z. Chen, Z. Li, and Y. Xu, “Spacetime gaussian feature splatting for real-time dynamic view synthesis,” in *Proceedings of the IEEE/CVF Conference on Computer Vision and Pattern Recognition (CVPR)*, June 2024, pp. 8508–8520.

[35] Z. Yang, H. Yang, Z. Pan, and L. Zhang, “Real-time photorealistic dynamic scene representation and rendering with 4d gaussian splatting,” in *The Twelfth International Conference on Learning Representations*, 2024.

[36] Y. Wang, P. Yang, Z. Xu, J. Sun, Z. Zhang, Y. Chen, H. Bao, S. Peng, and X. Zhou, “Freetimegs: Free gaussian primitives at anytime anywhere for dynamic scene reconstruction,” in *CVPR*, 2025.

[37] X. Zhang, Z. Liu, Y. Zhang, X. Ge, D. He, T. Xu, Y. Wang, Z. Lin, S. Yan, and J. Zhang, “Mega: Memory-efficient 4d gaussian splatting for dynamic scenes,” *arXiv preprint arXiv:2410.13613*, 2024.

[38] M. Lee, B. Lee, L. Y. Lee, E. Lee, S. Kim, S. Song, J. C. Lee, J. H. Ko, J. Park, and E. Park, “Optimized minimal 4d gaussian splatting,” 2025.

[39] G. Wu, T. Yi, J. Fang, L. Xie, X. Zhang, W. Wei, W. Liu, Q. Tian, and X. Wang, “4d gaussian splatting for real-time dynamic scene rendering,” in *Proceedings of the IEEE/CVF Conference on Computer Vision and Pattern Recognition (CVPR)*, June 2024, pp. 20310–20320.

[40] Z. Yang, X. Gao, W. Zhou, S. Jiao, Y. Zhang, and X. Jin, “Deformable 3d gaussians for high-fidelity monocular dynamic scene reconstruction,” in *2024 IEEE/CVF Conference on Computer Vision and Pattern Recognition (CVPR)*, 2024, pp. 20331–20341.

[41] Z. Guo, W. Zhou, L. Li, M. Wang, and H. Li, “Motion-aware 3d gaussian splatting for efficient dynamic scene reconstruction,” *IEEE Transactions on Circuits and Systems for Video Technology*, vol. 35, no. 4, pp. 3119–3133, 2025.

[42] H. Li, S. Li, X. Gao, A. Batuer, L. Yu, and Y. Liao, “Gifstream: 4d gaussian-based immersive video with feature stream,” in *Proceedings of the Computer Vision and Pattern Recognition Conference*, 2025, pp. 21761–21770.

[43] P. Dai, P. Zhang, Z. Dong, K. Xu, Y. Peng, D. Ding, Y. Shen, Y. Yang, X. Liu, R. W. H. Lau, and W. Xu, “4d gaussian videos with motion layering,” *ACM Trans. Graph.*, vol. 44, no. 4, 2025.

[44] J. Ballé, D. Minnen, S. Singh, S. J. Hwang, and N. Johnston, “Variational image compression with a scale hyperprior,” in *International Conference on Learning Representations*, 2018.

[45] H. Chen, B. He, H. Wang, Y. Ren, S. N. Lim, and A. Shrivastava, “Nerv: Neural representations for videos,” *Advances in Neural Information Processing Systems*, vol. 34, pp. 21557–21568, 2021.

[46] C. Gomes, R. Azevedo, and C. Schroers, “Video compression with entropy-constrained neural representations,” in *2023 IEEE/CVF Conference on Computer Vision and Pattern Recognition (CVPR)*, 2023, pp. 18497–18506.

[47] S. R. Maiya, S. Girish, M. Ehrlich, H. Wang, K. S. Lee, P. Poirson, P. Wu, C. Wang, and A. Shrivastava, “Nirvana: Neural implicit representations of videos with adaptive networks and autoregressive patch-wise modeling,” in *2023 IEEE/CVF Conference on Computer Vision and Pattern Recognition (CVPR)*, 2023, pp. 14378–14387.

[48] X. Zhang, R. Yang, D. He, X. Ge, T. Xu, Y. Wang, H. Qin, and J. Zhang, “Boosting neural representations for videos with a conditional decoder,” in *The IEEE/CVF Conference on Computer Vision and Pattern Recognition*, 2024.

- [49] H. M. Kwan, G. Gao, F. Zhang, A. Gower, and D. Bull, “Nvrc: Neural video representation compression,” *Advances in Neural Information Processing Systems*, vol. 37, pp. 132 440–132 462, 2024.
- [50] J. Wang, X. Zhang, G. Zhang, J. Zhu, L. Tang, and L. Zhang, “Uar-nvc: A unified autoregressive framework for memory-efficient neural video compression,” *IEEE Transactions on Circuits and Systems for Video Technology*, pp. 1–1, 2025.
- [51] H. Thomas, C. R. Qi, J.-E. Deschaud, B. Marcotegui, F. Goulette, and L. J. Guibas, “Kpconv: Flexible and deformable convolution for point clouds,” in *Proceedings of the IEEE/CVF international conference on computer vision*, 2019, pp. 6411–6420.
- [52] G. J. Sullivan, J.-R. Ohm, W.-J. Han, and T. Wiegand, “Overview of the high efficiency video coding (hevc) standard,” *IEEE Transactions on Circuits and Systems for Video Technology*, vol. 22, no. 12, pp. 1649–1668, 2012.
- [53] J. Lee, C. Won, H. Jung, I. Bae, and H.-G. Jeon, “Fully explicit dynamic gaussian splatting,” in *Proceedings of the Neural Information Processing Systems*, 2024.
- [54] T. Li, M. Slavcheva, M. Zollhoefer, S. Green, C. Lassner, C. Kim, T. Schmidt, S. Lovegrove, M. Goesele, R. Newcombe, and Z. Lv, “Neural 3d video synthesis from multi-view video,” in *2022 IEEE/CVF Conference on Computer Vision and Pattern Recognition (CVPR)*, 2022, pp. 5511–5521.
- [55] L. Li, Z. Shen, Z. Wang, L. Shen, and P. Tan, “Streaming radiance fields for 3d video synthesis,” in *Advances in Neural Information Processing Systems*, S. Koyejo, S. Mohamed, A. Agarwal, D. Belgrave, K. Cho, and A. Oh, Eds., vol. 35. Curran Associates, Inc., 2022, pp. 13 485–13 498.
- [56] F. Mentzer, E. Agustsson, M. Tschannen, R. Timofte, and L. Van Gool, “Practical full resolution learned lossless image compression,” in *Proceedings of the IEEE Conference on Computer Vision and Pattern Recognition (CVPR)*, 2019.
- [57] Z. Wang, A. Bovik, H. Sheikh, and E. Simoncelli, “Image quality assessment: from error visibility to structural similarity,” *IEEE Transactions on Image Processing*, vol. 13, no. 4, pp. 600–612, 2004.
- [58] G. Bjontegaard, “Calculation of average psnr differences between rd-curves,” *ITU SG16 Doc. VCEG-M33*, 2001.